A Theoretical Study on the Potential Energy Surface of the 1C3 + NO Reaction

ARTICLE *in* JOURNAL OF MOLECULAR STRUCTURE THEOCHEM · OCTOBER 2005

Impact Factor: 1.37 · DOI: 10.1016/j.theochem.2005.06.019

ELSEVIER

Journal of Molecular Structure: THEOCHEM 730 (2005) 207–215

THEO CHEM

www.elsevier.com/locate/theochem

A Theoretical Study on the Potential Energy Surface of the $^1C_3$ + NO Reaction

Ji-lai Li, Xu-ri Huang*, Hong-tao Bai, Cai-yun Geng, Guang-tao Yu, Chia-chung Sun

State Key Laboratory of Theoretical and Computational Chemistry, Institute of Theoretical Chemistry, Jilin University, Changchun 130023, People's Republic of China

Received 4 April 2005; revised 28 May 2005; accepted 18 June 2005
Available online 9 August 2005

Abstract

The reaction of linear form carbon cluster C_3 molecules in their $^1\Sigma$ ground state with NO ($X^2\Pi$) radicals is explored theoretically to investigate the formation of hitherto undetected NCCCO molecules in the interstellar medium via a neutral-neutral reaction. The doublet potential energy surface is worked out by the ab initio MO calculations at the CCSD(T)/cc-pVTZ//B3LYP/6-311G(d,p)+ZPE level of theory. It is shown that the main pathway of the $C_3(^1\Sigma)+NO(X^2\Pi)$ reaction involves the N-atom of NO attacking the side C-atom of the $^1C_3$ molecule first to form the adduct CCCNO, followed by the N-shift to give I6 CCNCO, and then to the main products P_1 (CCN+CO). Alternatively, I6 can be converted via the N-shift again to I9 (CN)CCO, and then it leads to the minor products P_2 (CNC+CO) and P_3 NCCCO. Since the three pathways have zero threshold energy and proceed via strongly bound energized complexes, they should possess the character of negative temperature dependence, and might be quite rapid even at very low temperature. The reaction represents facile neutral-neutral pathways to produce hitherto undetected CCN, CNC and NCCCO molecules in interstellar environments.

Keywords: Potential energy surface; Carbon cluster; Isomers

1. Introduction

Nitrogen, carbon, and oxygen chemistry have received considerable attention in various fields. One of the particular interests is their important roles in astrophysical chemistry. Up to now, nearly 125 nitrogen-, carbon-, sulfur-, silicon-, or oxygen-containing molecules have been detected in the interstellar space [1]. Interstellar molecules and possible potential ones, such as C*n* [2–12], HC*n* [4,13–15], C*n*N [4,13–18], C*n*O [4,13,19–20], HC*n*N [4,16,21–23] and FeO [24] metalline oxide, have been studied theoretically and/or experimentally in the last decades. Recently, Dua S. reported the syntheses of a number of stellar and potential stellar heterocumulene molecules in collision cells of a mass spectrometer [25], some of which may be precursors of systems of biological importance. One of the interesting features of some heterocumulene neutrals is that when energized, rearrangements of both the heteroatom and the carbon chain may occur: for example, C_2COC_2 rearranges to the more stable C_4CO [26], while NCCCN rearranges to CNCCN and also scrambles the carbons [27]. This suggests that when molecules of this type are formed in either interstellar dust clouds or circumstellar envelopes, there is the potential for rearrangement of such molecules to other isomers [28]. NC_3O, observed in mass spectrometers [29–31] during experiments, is one of the most interesting potential stellar molecules, and theoretical investigation suggests that neutral radical NCCCO isomer is most stable energetically [25,30], a comparison with the pentaatomic molecules NC_3S, SiC_3N and SiC_3P studied previous theoretically by us [32–34]. May NC_3O isomers rearrange to NCCCO when energized?

In the recent years, crossed molecular beam experiments demonstrated explicitly that neutral-neutral reactions can synthesize complex, carbon-bearing molecules in cold molecular clouds, as well as in outflow of carbon-rich asymptotic giant branch stars [35–39]. These reactions proceed mainly via an initial collision between the reactants, for example, a carbon or a radical attacking the carbon-carbon double or triple bond, and an adduct complex is

* Corresponding author. fax: +86 431 894 5942.
E-mail address: lijilai2008@yahoo.com (X.-r. Huang).

0166-1280/$ - see front matter © 2005 Elsevier B.V. All rights reserved.
doi:10.1016/j.theochem.2005.06.019

formed. Since the $C(^3P_j)/C_2H_2$ system [40] was found to reproduce the relative abundances of cyclic and linear C_3H isomers in the cold molecular cloud TMC-1 [41] and in the circumstellar envelope of the carbon star IRC+10216 [42], it is worthwhile to investigate whether the reaction of interstellar tricarbon molecules C_3 with nitric oxide NO could form the hitherto undetected interstellar molecules NC_3O via a neutral-neutral reaction,

$$C_3(X^1\Sigma g^+) + NO(X^2\Pi) \rightarrow NCCCO(X^2P)$$

$C_3(X^1\Sigma g^+)$, linear form of carbon cluster tricarbon molecule plays an important role in interstellar chemistry as well as in laboratory experiments. The tricarbon $C_3(X^1\Sigma g^+)$ molecules were found to be ubiquitous toward the Galactic center, hot core source Sagittarius B2 [43,44], in the well-studied dark cold cloud source TMC-1[45], and in the circumstellar shell of carbons stars such as IRC+10216 [44,46]. Optical emission from C_3 was detected in comet tails and coma [3,47–48] as well. In addition, C_3 might play a crucial role in diamond growth [49]. On the other hand, the nitric oxide radical, isoelectronic with HCO, is one of the most abundant nitrogenated molecule so far detected at millimeter wavelengths. As a fairly abundant interstellar molecule, NO has been identified in the cold molecular cloud TMC-1 [50], in Sagittarius B2, OCM1, W51, SgrA giant clouds [51–53] as well. Moreover, NO was detected firstly by McGonagle in the cold dark cloud L134N [53,54], and Gaur predicted NO may also be present in the sunspots through theoretical calculation [55]. Therefore, the reaction of C_3 with NO might form NC_3O isomers in those regions where both reactants exist. In this paper, we report a detailed high level ab initio study of potential energy surface(PES) for this reaction, the thermodynamic properties and molecular structures of its intermediates, products, and transition states, elucidate the mechanism of the reaction, and consider astrophysical implications which follows. Some of conclusions drawn in this work may be helpful for further experimental study of this reaction.

2. Computational methods

The calculations reported in the present study were carried out using the density functional theory (DFT) functional B3LYP(the hybrid three-parameter functional developed by Becke) [56–58], as implemented in the Gaussian98 program package [59]. Tran K. M. et al. have previously reported the success of the B3LYP method in predicting geometries of unsaturated chain structures, and this method produces optimized structures, at low computational cost, that compared favorably with higher level calculations [19]. The geometries were optimized by calculating the force constants at every point with basis set 6-311G(d,p), and no symmetry constraints. Using the same level of theory, vibrational frequency calculations verified the identity of each stationary point as a minimum or transition state. Transition structures were characterized by a single imaginary frequency while minimum structures have no imaginary frequency. Specially, intrinsic reaction coordinate calculations were performed to connect the transition states to their respective minima [60]. Zero-point vibrational energy corrections have been applied, but have not been scaled. In order to obtain more reliable energy, the coupled-cluster CCSD(T) method with single, double, and perturbative treatment of triple excitations [61] in conjunction with the correlation-consistent polarized valence triple-ζ basis sets cc-pVTZ [62] was used. The B3LYP/6-311G(d,p) optimized geometries were used for the single-point coupled cluster calculations without reoptimization at the CCSD(T) /6-311G(d,p) or CCSD(T)/cc-pVTZ levels. All calculations were carried out on the SGI O3800 Servers.

3. Results and discussion

There are two stable forms of C_3, viz. the $^1\Sigma$ linear ground state and the $^3\Sigma$ linear triple state. Since $C_3(^3\Sigma)$ is 61.42 kcal·mol^{-1} less stable than $C_3(^1\Sigma)$ at the CCSD(T) /cc-pVTZ//B3LYP/6-311G(d,p)+ZPE level of theory, the reaction of the triple state $^3C_3$ with NO hasn't been considered further. Considering the quartet PESs in our previous investigations [5,12] on the reactions of $^3C_2+NO$ and $^3C_2+NO_2$ have less competitive abilities than the doublet PESs and even they can be neglected, the quartet PES hasn't been considered in this present.

A total of fourteen minimum intermediate isomers and twenty-five transition states are located and a variety of possible pathways are probed. The optimized structural parameters of the reactants, intermediates and the products of the reaction are shown in Fig. 1. The optimized structural parameters of the transition states on the doublet electronic state are shown in Fig. 2. Schematic plots of the relative energies of the doublet potential energy surface (PES) are shown in Fig. 3. The dissociation curve with respect to the dissociation of the C–N bond in I1 CCCNO (for conciseness, intermediate 'n' in the latter is simplified as 'In' in this paper, where n is the serial number of the intermediate) is shown in Fig. 4a. Total energies of all the species involved in the reaction are listed in Table 1. The vibrational frequencies and dipole moment of NCCCO, CCN and CNC are compiled in Table 2, respectively.

As the kinetic and thermodynamic stability of intermediate NCCCO, we look on it as one of the products, P_3. As shown in Fig. 3, the dissociation of the four internal bonds of P_3 can proceed barrierlessly to form P_{3a} (NCCC + O), P_1(NCC + CO), P_{3b} (NC + CCO), and P_{3c} (N+ CCCO), respectively. Their direct dissociation curves via point-wise optimization method are shown in Fig. 4b.

There are two distinguishable reaction mechanisms involved on the $^1C_3+NO$ reaction on the doublet PES, i. e. the N-atom attacking mechanism and O-atom attacking

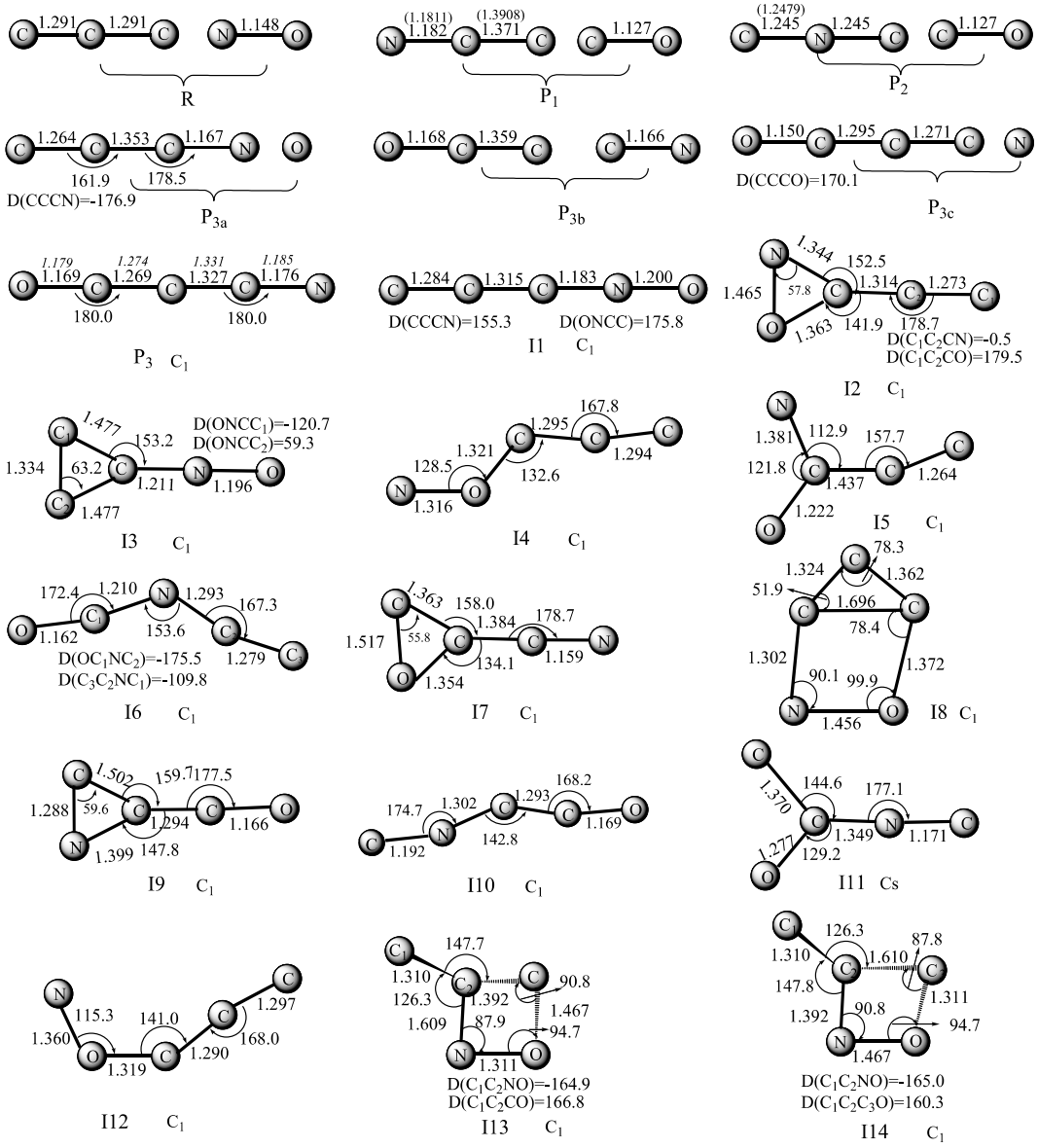

Fig. 1. Optimized geometries of reactants, intermediate isomers and products at the UB3LYP/6-311G(d,p) level of theory. Important bond distances are given in angstroms, bond angles in degrees. The numbers in italics show B3LYP/6-31G(d) optimized geometric parameters[25]. The numbers in parentheses show CCSD(T)/TZ2P optimized geometric parameters[21].

mechanism. The N-atom attacking mechanism is the N-atom of the nitric oxide radical attack the linear form of carbon cluster $^1C_3$ including N-atom on side and/or middle C-atom of $^1C_3$ in the first step of the reaction to produce I1 directly and/or I3 via transition state $TS_{R\text{-}3}$. And that the O-atom attacking mechanism is the O-atom of nitric oxide attack the side C-atom of the $^1C_3$ molecule in the first step of the reaction to produce I4 via the transition state TSR-4.

3.1. A N-atom attacking mechanism

The N-atom attacking mechanism can be divided into two individual sub-mechanisms according to the different sites of the $^1C_3$ molecule that the N-atom of nitric oxide attacks. The sub-mechanism I starts from the N-atom of nitric oxide attacking the side C-atom of $^1C_3$ molecule directly forming the adduct I1 CCCNO with large heat (35.28 kcal·mol^{-1}) released in the first reaction step. Whereas the sub-mechanism II is that the N-atom of nitric oxide attacks the middle C-atom of the $^1C_3$ molecule in the first reaction step, forming I3(-10.41) via $TS_{R\text{-}3}$(14.56).

3.1.1. a. Sub-mechanism I

As shown in Fig. 3, this is a barrierlessly exothermic step with the reaction energy of −35.28 kcal·mol^{-1} at the CCSD(T)/cc-pVTZ//B3LYP/6-311G(d,p)+ZPE level of theory. At the UB3LYP/6-311G(d,p) level, we are not able to locate any addition transition states from R to I1.

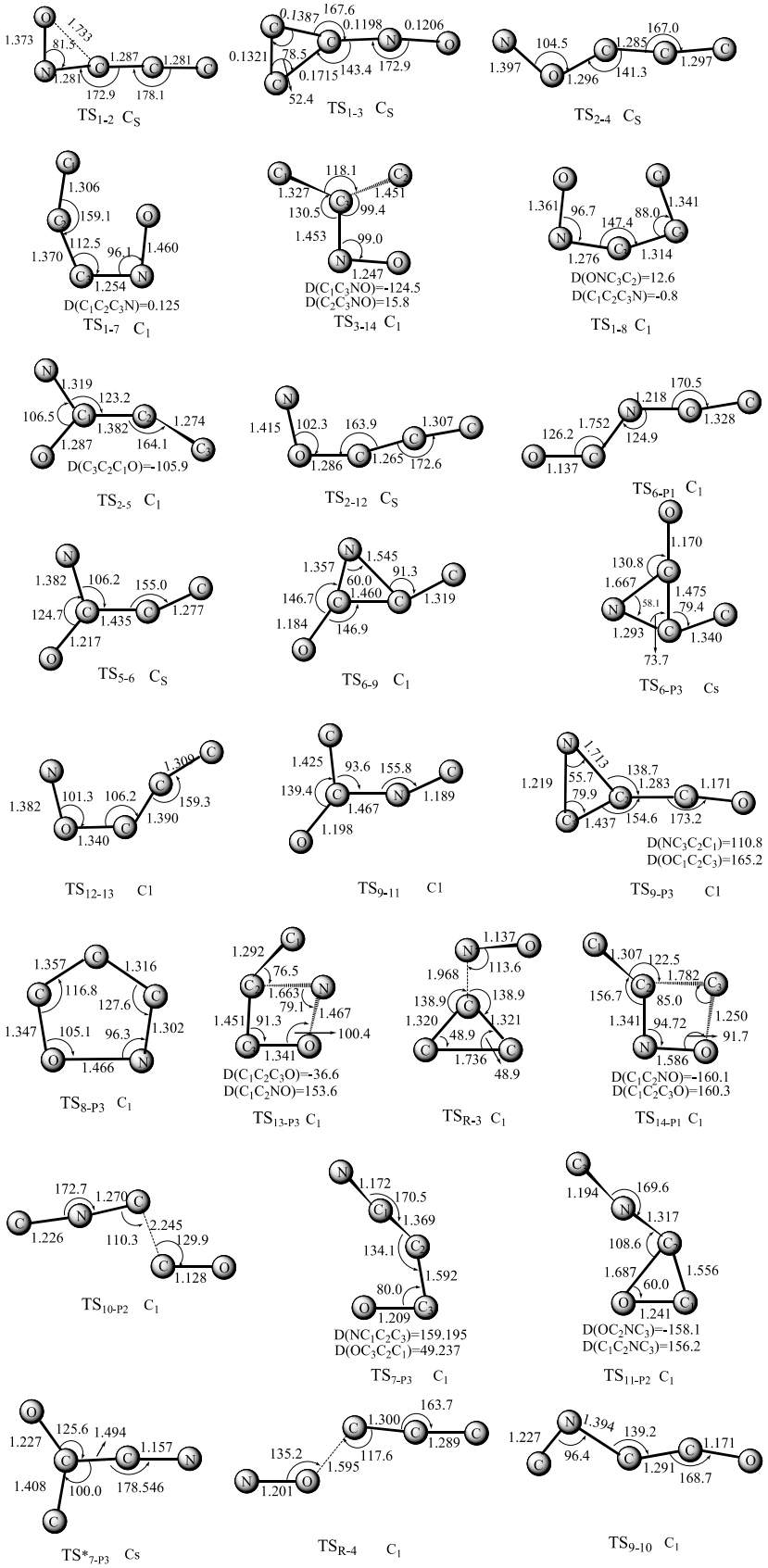

Fig. 2. Optimized geometries of transition states at the B3LYP/6-311G(d,p) level of theory. Important bond distances are given in angstroms, bond angles in degrees.

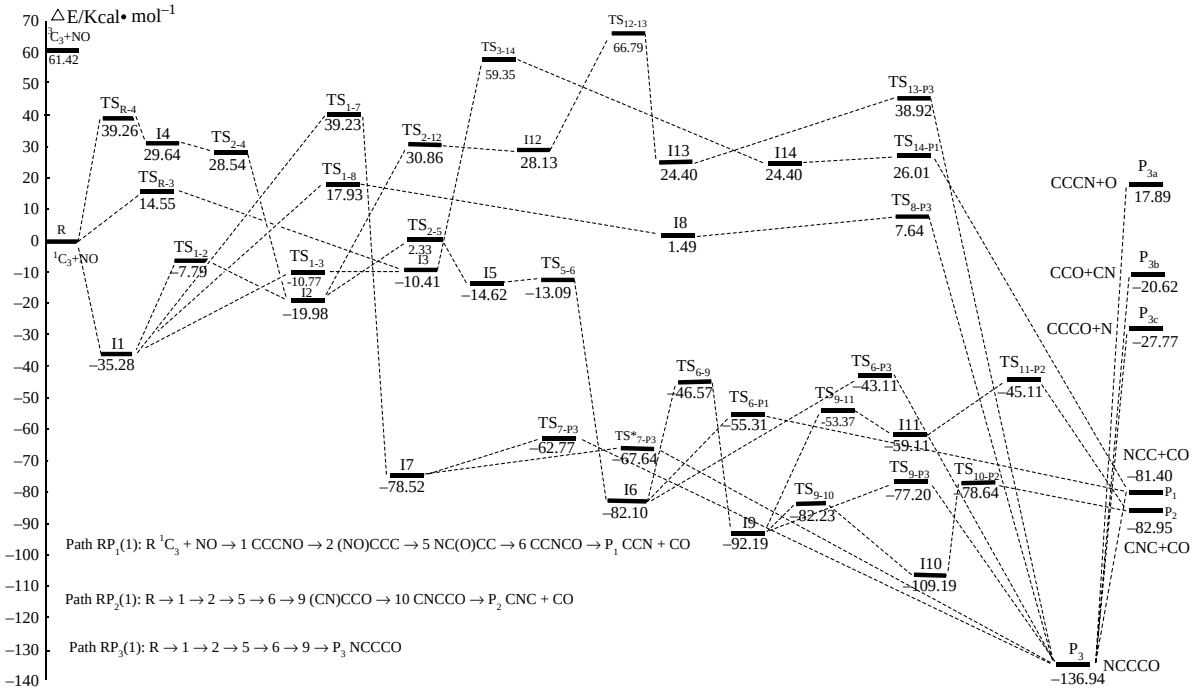

Fig. 3. Schematic pathways for the $^1C_3+NO$ reaction relative energies are calculated at the CCSD(T)/cc-pVTZ//B3LYP/6-311G(d,p)+ZPE level of theory.

Indeed, the dissociation curve of the C—N bond in I1 to approach the reactants is worked out via point-wise optimization method, that is, we calculate the energy by changing the atom distance point by point while the remaining geometrical parameters are fully optimized with each point. From Fig. 4a, we can clearly see that the energy of the complex ON···CCC increases point by point from the equilibrium geometry I1 as the distance between the side C-atom and the N-atom increases. On account of not finding a 'hill' (character of transition state) on the curve in the region of 1.6–2.5 Å(distance-axis), we therefore expect that the N-atom may directly adduct to the side C-atom of $^1C_3$ to form I1. Clearly, I1 is an energy-rich species and may make the reaction easier to go through the subsequent reaction steps. From the I1, there are nine isomerization and dissociation pathways that can be expressed as follows:

Path $RP_1(1)$: R $^1C_3+NO \rightarrow 1$ CCCNO $\rightarrow 2$ (NO)CCC $\rightarrow$ 5 NC(O)CC $\rightarrow 6$ CCNCO $\rightarrow P_1$ CCN + CO

Path $RP_2(1)$: R $\rightarrow 1 \rightarrow 2 \rightarrow 5 \rightarrow 6 \rightarrow 9$ (CN)CCO $\rightarrow 10$ CNCCO $\rightarrow P_2$ CNC + CO

Path $RP_3(1)$: R $\rightarrow 1 \rightarrow 2 \rightarrow 5 \rightarrow 6 \rightarrow 9 \rightarrow P_3$ NCCCO

Path $RP_2(2)$: R $\rightarrow 1 \rightarrow 2 \rightarrow 5 \rightarrow 6 \rightarrow 9 \rightarrow 11$ CC(O)NC $\rightarrow P_2$

Path $RP_3(2)$: R $\rightarrow 1 \rightarrow 2 \rightarrow 5 \rightarrow 6 \rightarrow P_3$

Path $RP_3(3)$: R $\rightarrow 1 \rightarrow 8$ c-NOC(C)C $\rightarrow P_3$

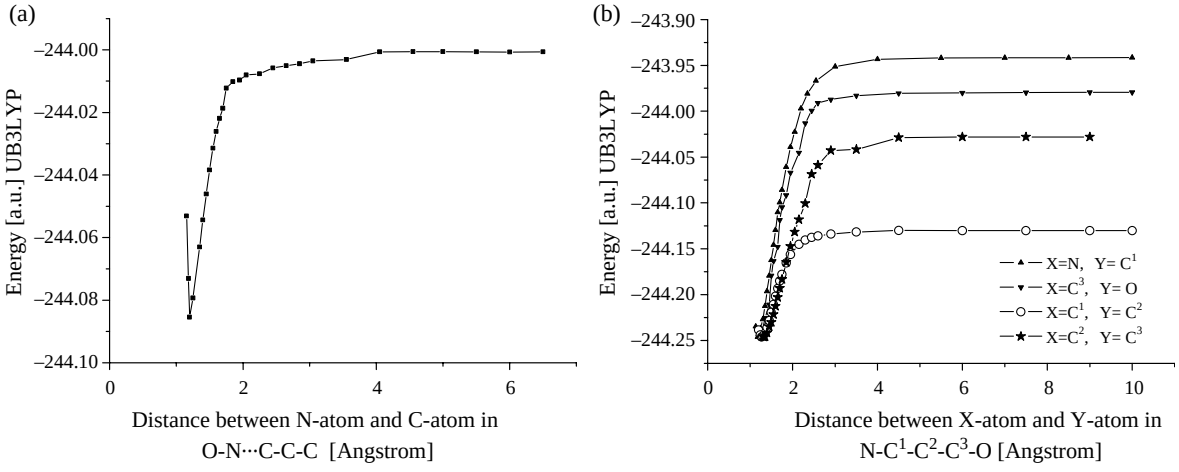

Fig. 4. Bond dissociation curves calculated via point-wise optimized method at the UB3LYP/6-311G(d,p) level of theory. (a) Dissociation curve with respect to the dissociation of the C–N bond in the I1 (CCCNO); b). Dissociation curve with respect to the dissociation of the X—Y bond in the $P_3(NC^1C^2C^3O)$.

Table 1
Theoretical predication of the total energy(Hartree), ZPE(Hartree/particle), and relative energies(kcal·mol^{-1}) for products, intermediate isomers and transition states of C_3+NO at different levels of theory

Species	ZVPE	B3LYP/6-311G(d,p)	CCSD(T)/6-311G(d,p)	CCSD(T)/cc-pvtz	RE[a]	RE[b]
$R(C_3+NO)$	0.012486	−244.000665	−243.411819	−243.5494749	0	0.00
$^3C_3+NO$	0.009616	−243.9206694	−243.3158184	−243.4515931	58.44	61.42
1	0.018267	−244.085976	−243.466088	−243.6114789	−30.43	−35.28
2	0.017150	−244.036303	−243.440047	−243.5859792	−14.79	−19.98
3	0.016492	−244.039913	−243.428134	−243.5700701	−7.72	−10.41
4	0.015012	−243.975725	−243.363876	−243.5047655	31.67	29.64
5	0.015736	−244.036303	−243.437745	−243.5760248	−14.23	−14.62
6	0.019226	−244.164199	−243.550526	−243.6870489	−82.81	−82.10
7	0.017612	−244.134879	−243.536049	−243.6797355	−74.74	−78.52
8	0.018203	−244.003653	−243.403901	−243.5528165	8.56	1.49
9	0.018442	−244.167172	−243.559828	−243.7023487	−89.14	−92.19
10	0.019043	−244.198225	−243.587317	−243.7300406	−106.01	−109.19
11	0.017344	−244.104883	−243.504869	−243.6485268	−55.34	−59.11
12	0.015026	−243.973405	−243.366074	−243.5071905	30.30	28.13
13	0.015346	−243.967518	−243.368153	−243.5134536	29.20	24.40
14	0.015344	−243.967518	−243.368153	−243.5134539	29.19	24.40
P_1	0.012737	−244.130276	−243.544364	−243.6794523	−83.02	−81.40
P_2	0.011988	−244.133454	−243.546693	−243.6811732	−84.95	−82.95
P_3	0.019901	−244.246235	−243.632654	−243.7751101	−133.92	−136.94
P_{3a}	0.013449	−243.979210	−243.3881228	−243.5219356	15.47	17.89
P_{3b}	0.012898	−244.038003	−243.4466456	−243.5827509	−21.60	−20.62
P_{3c}	0.015128	−244.045173	−243.417040	−243.596395	−1.62	−27.77
TS_{1-2}	0.016090	−244.033056	−243.419591	−243.5654959	−2.62	−7.79
TS_{2-5}	0.014777	−244.019311	−243.407104	−243.5480445	4.40	2.33
TS_{5-6}	0.015420	−244.036142	−243.434507	−243.5732666	−12.40	−13.09
$TS_{6\text{-}P1}$	0.015244	−244.108030	−243.504829	−243.6403774	−56.63	−55.31
TS_{1-7}	0.014897	−243.941973	−243.335699	−243.4893741	49.28	39.23
TS_{1-8}	0.015791	−243.978075	−243.376838	−243.5241042	24.02	17.93
$TS_{8\text{-}P3}$	0.017194	−243.998767	−243.395133	−243.542012	13.42	7.64
$TS_{R\text{-}3}$	0.013645	−243.982958	−243.387824	−243.5274443	15.78	14.55
TS_{3-14}	0.014164	−243.918086	−243.313364	−243.4565688	62.83	59.35
TS_{14-P1}	0.014026	−243.964521	−243.364299	−243.5095726	30.79	26.01
TS_{1-3}	0.016268	−244.038497	−243.425081	−243.5704253	−5.95	−10.77
$TS_{R\text{-}4}$	0.013271	−243.962418	−243.347602	−243.4876926	40.79	39.26
TS_{2-4}	0.014663	−243.971762	−243.364676	−−243.5061765	30.95	28.54
TS_{2-12}	0.014340	−243.970353	−243.360241	−243.5021573	33.55	30.86
TS_{12-13}	0.013932	−243.929979	−243.324974	−243.4448727	55.40	66.53
$TS_{13\text{-}P3}$	0.014481	−243.938208	−243.342549	−243.4894447	44.72	38.92
TS_{6-9}	0.016663	−244.084521	−243.483996	−243.6278716	−42.67	−46.57
TS_{9-10}	0.017011	−244.148824	−243.543016	−243.6850442	−79.49	−82.23
TS_{6-P3}	0.016403	−244.076342	S243.478029	−243.6220929	−39.09	−43.11
$TS_{7\text{-}P3}$	0.015212	−244.110927	−243.514901	−243.6522266	−62.97	−62.77
$TS^*_{7\text{-}P3}$	0.016361	−244.116813	−243.520285	−243.6611333	−65.63	−67.64
TS_{9-11}	0.015907	−244.094346	−243.496677	−243.6379463	−51.10	−53.37
$TS_{10\text{-}P2}$	0.014166	−244.132451	−243.540184	−243.6764681	−79.50	−78.64
$TS_{9\text{-}P3}$	0.016991	−244.141254	−243.534443	−243.6770044	−74.12	−77.20
$TS_{11\text{-}P2}$	0.015056	−244.080418	−243.483169	−243.6239357	−43.16	−45.11

[a] RE[a] represents the relative energies calculated at CCSD(T) /6-311G(d,p)// B3LYP/6-311G(d,p) + ZPE level of theory.
[b] RE[b] represents the relative energies calculated at CCSD(T)/cc-pVTZ// B3LYP/6-311G(d,p) + ZPE level of theory.

Path $RP_3(4)$: R→1→7 (CO)CCN→P_3
Path $RP_1(2)$: R→1→3 (CC)CNO→14 C-c-CNOC→P_1
Path $RP_3(5)$: R→1→2→12 NOCCC→13 C-c-CNOC→P_3

Obviously, for the first five pathways of the sub-mechanism I, they possess the same initial steps of the reaction, i.e. R→1→2→5→6. It is a N-adduct-shift mechanism. The difference of the five pathways is the way how I6 CCNCO changes to P_1, P_2 and P_3. From I6 CCNCO (−82.10), pathway $RP_1(1)$ can reach the products P_1 (CCN+CO) easily via overcoming the transition state $TS_{6\text{-}p1}$ (−55.31), a 26.79 kcal·mol^{-1} energy barrier. For pathway $RP_2(1)$, I6 transforms to P_2 by going through TS_{6-9}(−46.57), I9(−92.19), TS_{9-10}(−82.23), I10(−109.19), and $TS_{10\text{-}p2}$(−78.64) respectively. Because it possesses

Table 2
Theoretical calculations of the dipole moments and vibrational frequencies of relevant isomers

Species	State	Dipole Moment/D	Vibrational Frequencies (cm^{-1})
NCCCO	$X^2\Pi$	1.6910 1.63[a]	2220.5 (702.4), 2089.4(0.1), 1603.3(34.6), 748.3(0.1), 560.1(17.0) 534.2(1.4), 489.6(39.6), 467.8(1.1), 136.7(6.5), 18.7(0.0)
CCN	$X^2\Pi$	0.1324 0.1328[b]	2018.5(111.1), 1078.3(71.5), 339.4(22.0) **1923**, **1051**, **325**
CNC	$X^2\Pi$	0.00	1504.3(48.5), 1299.6(0.0), 317.5(7.7) *1502.1 (48.4)*, *1298 (0.0)*, *318.5 (7.6)*

Note: Infrared intensities in $km \cdot mol^{-1}$ are given in parentheses. The numbers in bold are experimental data reported by N. Oliphant [69] and in italics are reported by A.M. Mebel [21]. (a). At B3LYP/6-31G(d) level of theory from ref. [25]. (b). At CCSD(T)/TZ2P level of theory from ref. [21].

a 35.53 $kcal \cdot mol^{-1}$ energy barrier, pathway $RP_2(1)$ should be less competitive than pathway $RP_1(1)$ in low-temperature range. As shown in Fig. 3, P_3 dissociates barrierlessly to four educts, i.e. P_1, P_{3a}, P_{3b}, and P_{3c}, and their energies above P_3 are 55.54, 109.17, 116.32 and 154.83 $kcal \cdot mol^{-1}$ respectively. The direct dissociation curves of P_3 to the educts were confirmed via point-wise optimization method mentioned above (see Fig. 4b). From Fig. 4b and Table 1, we can safely draw the conclusion that P_3 has more kinetic and thermodynamic stability than other isomers and products. The dissociation of P_3 will not be discussed in kinetics mechanism analysis. Pathway $RP_3(1)$ has the same step of $6 \rightarrow 9$ as pathway $RP_2(1)$. I9 transforms to P_3 via transition state $TS_{9\text{-}p3}$ (-77.20), a 14.99 $kcal \cdot mol^{-1}$ energy barrier. Although the energy barrier (transition state $TS_{9\text{-}p3}$) in pathway $RP_3(1)$ is slightly higher than that (transition state $TS_{10\text{-}p2}$) in pathway $RP_2(1)$, we expect that the former pathway may be not less competitive than the latter for the sake of the kinetic and thermodynamic stability of P_3 in high-temperature range. As temperature increases, the handicap of energy barrier will be weakened. Therefore, the pathway $RP_3(1)$ may be more favorable than $RP_2(1)$ to a degree in high-temperature range. Pathway $RP_2(2)$ has the same step of $6 \rightarrow 9$ as pathways $RP_2(1)$ and $RP_3(1)$ as well. While in pathway $RP_2(2)$, I9 (CN)CCO transforming to P_2 will overcome a 47.08 $kcal \cdot mol^{-1}$ energy barrier. It is not difficult to draw the conclusion that pathway $RP_2(2)$ is less competitive than pathway $RP_2(1)$ and $RP_3(1)$ because of the high relative energy barrier. Analogously, in pathway $RP_3(2)$, I6 converted to product P_3, the energy barrier of transition state $TS_{6\text{-}p3}$ (-43.11) is the highest energetic species between I6 and the products among all the five pathways mentioned above. Tell its own tale, the pathway $RP_3(2)$ may be least competitive kinetically among the $RP_1(1)$, $RP_2(1)$, $RP_3(1)$, $RP_2(2)$, and $RP_3(2)$ pathways in low-temperature range. Since only the relative energy of transition state $TS_{2\text{–}5}$ (2.33) in the five pathways discussed above is slight higher than that of the reactants (0.00), the rate of these pathways should be determined by the arrangement of I2 (NO)CCC to I5 O(N)CCC, which is a stepwise process and will process if the energy barrier of 2.33 $kcal \cdot mol^{-1}$ can be surmounted. As can be seen from Table 1, the relative energy of I6 is much lower than that of the I1, so I6 may make the subsequent steps of the reaction proceed more easily. Furthermore, since the five pathways have zero threshold energy and proceed via strongly bound energized complexes, they should possess the character of negative temperature dependence, and might be quite rapid even at very low temperature [63].

There are other four pathways else in the sub-mechanism I except for the five pathways discussed above, i.e. pathways $RP_3(3)$, $RP_3(4)$, $RP_1(2)$ and $RP_3(5)$. The pathway $RP_3(3)$ is much more favorable than the other pathways because the energy barrier 17.93 $kcal \cdot mol^{-1}$ of the transition state $TS_{1\text{–}8}$ is lower than those energy barriers 39.23, 59.35 and 66.79 $kcal \cdot mol^{-1}$ in pathways $RP_3(4)$, $RP_1(2)$ and $RP_3(5)$ respectively. It is easily seen that in pathway $RP_3(4)$ there are two transition states $TS_{7\text{-}p3}$ (-62.77) and $TS^{*}_{7\text{–}p3}$ (-67.64) whereas IRC calculations suggest that they link with the same stationary points on both sides the saddle points. As can be seen from Fig. 2, the two transition states are some alike. Furthermore, from Table 1 and Fig. 3, it is not difficult to find that, for the four pathways, pathways $RP_3(5)$ and $RP_1(2)$ possessing particularly high energies and high barriers then the pathways themselves lack of kinetically competitive abilities. Thus, we may conclude that the four pathways are the minor pathways.

Brief summary, pathways $RP_1(1)$, $RP_2(1)$ and $RP_3(1)$ are major pathways among all pathways mentioned above. The pathway $RP_1(1)$ is the most competitive pathway while pathway $RP_3(1)$ is least competitive among the three major pathways. In higher-temperature range, pathway $RP_3(1)$ may be more favorable than $RP_2(1)$ on the doublet PES.

3.1.2. Sub-mechanism II

For the first step of the reaction $R \rightarrow 3$, the N-atom of NO attacks the middle C-atom of the $^1C_3$ molecule to form I3 (CC)CNO (-10.41) via the transition state $TS_{R\text{-}3}$ with a high entrance barrier of 14.55 $kcal \cdot \ominus mol^{-1}$. There are two distinguishable second steps, $3 \rightarrow 1$ and $3 \rightarrow 14$, whose energy barrier heights are -0.36 $kcal \cdot mol^{-1}$ and 48.94 $kcal \cdot mol^{-1}$ respectively. Therefore, for pathway $RP_1(3)$: $R \rightarrow 3 \rightarrow 14 \rightarrow P_1$, the high energy barrier in the first and second steps in the sub-mechanism II may rule out its significance in astrophysical chemistry in lower- or higher-temperature range. Whereas, given the temperature considerable high, the reactants may overcome the barrier of $TS_{R\text{-}3}$ and give to

I1. Hereby, the pathways of the sub-mechanism II are homologous with the same steps of sub-mechanism I in general except for the reaction entrance. For conciseness, we only list them as follows:

Path $RP_1(3)$: $R \rightarrow 3 \rightarrow 14 \rightarrow P_1$
Path $RP_1(4)$: $R \rightarrow 3 \rightarrow 1 \rightarrow 2 \rightarrow 5 \rightarrow 6 \rightarrow P_1$
Path $RP_2(3)$: $R \rightarrow 3 \rightarrow 1 \rightarrow 2 \rightarrow 5 \rightarrow 6 \rightarrow 9 \rightarrow 10 \rightarrow P_2$
Path $RP_3(6)$: $R \rightarrow 3 \rightarrow 1 \rightarrow 2 \rightarrow 5 \rightarrow 6 \rightarrow 9 \rightarrow P_3$
Path $RP_2(4)$: $R \rightarrow 3 \rightarrow 1 \rightarrow 2 \rightarrow 5 \rightarrow 6 \rightarrow 9 \rightarrow 11 \rightarrow P_2$
Path $RP_3(7)$: $R \rightarrow 3 \rightarrow 1 \rightarrow 2 \rightarrow 5 \rightarrow 6 \rightarrow P_3$
Path $RP_3(8)$: $R \rightarrow 3 \rightarrow 1 \rightarrow 8 \rightarrow P_3$
Path $RP_3(9)$: $R \rightarrow 3 \rightarrow 1 \rightarrow 7 \rightarrow P_3$
Path $RP_3(10)$: $R \rightarrow 3 \rightarrow 1 \rightarrow 2 \rightarrow 12 \rightarrow 13 \rightarrow P_3$

It should be noted that the relative energy of TS_{1-3} is lower than that of I3, which the stationary point TS_{1-3} connected with through IRC calculation. The problem about the upside-down energies of TS_{1-3} and I3 lies in the theoretical computational method we adopted during the calculation. As introduced in the computational methods section all energies presented in the paper are at the CCSD(T)/6-311G(d,p)//B3LYP/6-311G(d,p)+ZPE or CCSD(T)/cc-pVTZ//B3LYP/6-311G(d,p)+ZPE level. If the potential energy barrier is very low and the ZPE correction is significant, this treatment of the energies can lead to a barrier less than zero. Because it has been suggested that DFT calculations can underestimate barriers' height by a few $kcal \cdot mol^{-1}$, such a situation should not be over-interpreted, but can be taken as an indication of the lack of a significant barrier.

3.2. B O-atom attacking mechanism

The nine pathways corresponding to the O-atom attacking mechanism of the $^1C_3+NO$ reaction on the doublet PES can be expressed as:

Path $RP_1(5)$: $R \rightarrow 4$ NOCCC $\rightarrow 2 \rightarrow 5 \rightarrow 6 \rightarrow P_1$
Path $RP_2(5)$: $R \rightarrow 4 \rightarrow 2 \rightarrow 5 \rightarrow 6 \rightarrow 9 \rightarrow 10 \rightarrow P_2$
Path $RP_3(11)$: $R \rightarrow 4 \rightarrow 2 \rightarrow 5 \rightarrow 6 \rightarrow 9 \rightarrow P_3$
Path $RP_2(6)$: $R \rightarrow 4 \rightarrow 2 \rightarrow 5 \rightarrow 6 \rightarrow 9 \rightarrow 11 \rightarrow P_2$
Path $RP_3(12)$: $R \rightarrow 4 \rightarrow 2 \rightarrow 5 \rightarrow 6 \rightarrow P_3$
Path $RP_3(13)$: $R \rightarrow 4 \rightarrow 2 \rightarrow 1 \rightarrow 8 \rightarrow P_3$
Path $RP_3(14)$: $R \rightarrow 4 \rightarrow 2 \rightarrow 1 \rightarrow 7 \rightarrow P_3$
Path RP1(6): $R \rightarrow 4 \rightarrow 2 \rightarrow 1 \rightarrow 3 \rightarrow 14 \rightarrow P_1$
Path $RP_3(15)$: $R \rightarrow 4 \rightarrow 2 \rightarrow 12 \rightarrow 13 \rightarrow P_3$

It is clear that the first two steps of the pathways on the PES are $R \rightarrow 4 \rightarrow 2$. In the first step of the reaction the O-atom attacks the side C-atom of the $^1C_3$ molecule to form I4 NOCCC via transition state $TS_{R\text{-}4}$, a 39.26 $kcal \cdot mol^{-1}$ energy barrier. I4 transforms to I2 by overcoming transition state TS_{2-4} (28.54), whose relative energy is lower than that of I4 (29.64). This phenomenon has been mentioned in *3. A* b section. Obviously, all of the pathways possess a considerable high energy barrier of 39.26 $kcal \cdot mol^{-1}$ in the first step of the reaction, which makes the subsequent steps of the reaction proceed impossible. Therefore, the O-atom attacking mechanism can be safely ruled out from the doublet PES.

4. Conclusions and implications

The mechanism of the $^1C_3+NO$ reaction is elucidated explicitly by means of ab initio calculations at the B3LYP/6-311G(d,p) level of theory. The major pathways in lower-temperature range are $RP_1(1)$, $RP_2(1)$ and $RP_3(1)$ on the doublet PES. The pathway $RP_1(1)$ is the most competitive pathway while pathway $RP_3(1)$ is least competitive among the three major pathways. In higher-temperature range, pathway $RP_3(1)$ may be more favorable than $RP_2(1)$ on the doublet PES. Other pathways on the doublet PES may be less competitive in this reaction in lower-temperature range. The title reaction represents facile neutral-neutral pathways to produce hitherto undetected CCN, CNC and NCCCO molecules in interstellar environments.

As demonstrated above, P_1 is expected to be the main product and the formation of P_3 molecules should be considerable favorableness in the interstellar medium via neutral-neutral reaction. This doesn't mean that CCN is more than NCCCO in space for two reasons. First, because CCN reacts with normal alkanes to form CH_2CHCN [64,65], and CH_2CHCN coexists with C_3 and NO in TMC-1 and Sagittarius B2 [66,67], it is reasonable to conclude that CCN may be depleted in this region. Second, as shown on the doublet PES, located in a deep energy well, NCCCO is very stable in thermodynamics and kinetics and difficult to dissociate once produced. $C(^3P_j)+HCN$ reaction [21] proved this nicely due to HCCN coexists with reactants C and HCN in IRC+10216 [68]. Therefore, it is safe to draw a conclusion that if a reaction exit barrier is very high on the PES, the most stable intermediate isomer may coexist with reactants and/or products.

Regarding a possible future search for interstellar NCCCO and C_2N isomers, it is further very interesting to compare the computed vibrational frequencies and dipole moments with previous data [21,25,69]. As shown in Table 2, the NCCCO radical has a dipole moment of 1. 691D while the CCN isomer has only a small dipole moment of 0.1324 D and CNC has no dipole moment, therefore the search for NCCCO via microwave spectroscopy is feasible but might be extremely challenging for CCN and impossible for CNC. Since further CNC depicts no pure rotational spectrum, a detection of both linear isomers in the infrared region might be advisable. All in all, it is more instructive to focus the detection on those regions carefully where both the reactants exist, such as Sagittarius B2.

Acknowledgements

This work is supported by the National Natural Science Foundation of China (nos. 20073014 and 20103003), Excellent Young Teacher Foundation of the Ministry of Education of China, Excellent Young Foundation of Jilin Province. The authors are greatly thankful for the reviewers' invaluable comments.

References

[1] For a list of the 125 molecules detected so far see: http://www.cv.nrao.edu/~awootten/allmols.html.
[2] J.V. Richard, Chem. Rev. 89 (1989) 1713.
[3] A. Van Orden, R.J. Saykally, Chem. Rev. 98 (1998) 2313.
[4] R.I. Kaiser, Chem. Rev. 102 (2002) 1309.
[5] Z.G. Wei, X.R. Huang, S.W. Zhang, Y.B. Sun, H.J. Qian, C.C. Sun, J. Phys. Chem. A 108 (2004) 6771.
[6] S.J. Blanksby, D. Schroder, S. Dua, J.H. Bowie, H. Schwarz, J. Am. Chem. Soc. 122 (2000) 7105.
[7] J. Kurtz, L. Adamowicz, Astrophys. J. Part 1 370 (1991) 784.
[8] A.M. Mebel, R.I. Kaiser, Chem. Phys. Lett. 360 (2002) 139.
[9] T. Kruse, P. Roth, Inc. Int J. Chem. Kinet. 31 (1999) 11.
[10] T.F. Giesen, A.O. Van Orden, J.D. Cruzan, R.A. Provencal, R.J. Saykally, Astrophys. J. 551 (2001) L181.
[11] A.G. Löwe, A.T. Hartlier, J. Brand, B. Atakan, Kohse-Höinghaus, Combust. Flame 118 (1999) 37.
[12] Z.G. Wei, X.R. Huang, Y.B. Sun, J.Y. Liu, C.C. Sun, J. Mol. Struct. (Theochem) 671 (2004) 133.
[13] S.J. Blanksby, J.H. Bowie, Mass Spectrom. Rev. 18 (1999) 131.
[14] C.A. Gottlieb, E.W. Gottlieb, P. Thaddeus, H. Kawamura, Astrophys. J. Part 1 275 (1983) 916.
[15] S. Green, Astrophys. J. Part 1 240 (1980) 962.
[16] T. Tatiana, B.H. Joshua, Chem. Phys. Lett. 323 (2000) 305.
[17] K. Chuchev, J.J. BelBruno, J. Phys. Chem. A 106 (2002) 4240.
[18] S. Wilson, S. Green, Astrophys. J. Part 2 212 (1977) L87.
[19] K.M. Tran, A.M. McAnoy, J.H. Bowie, Org. Biomol. Chem. 2 (2004) 999.
[20] J.C. Rienstra-Kiracofe, G.B. Ellison, B.C. Hoffman, H.F. Schaefer, J. Phys. Chem. A 104 (2000) 2273.
[21] A.M. Mebel, R.I. Kaiser, Astrophys. J. 564 (2002) 787.
[22] H.H. Lee1, E. Roueff, G. Pineau des Forets, O.M. Shalabiea, R. Terzieva, E. Herbst, Astron. Astrophys. 334 (1998) 1047.
[23] S. Petrie, J. Phys. Chem. A 106 (2002) 11181.
[24] M.D. Allen, L.M. Ziurys, J.M. Brown, Chem. Phys. Lett. 257 (1996) 130.
[25] S. Dua, J.H. Bowie, J. Chem. Soc. Perkin Trans. 2 (2001) 827.
[26] S. Dua, S.J. Blanksby, J.H. Bowie, Int. J. Mass Spectrom. 45 (2000) 195.
[27] S.J. Blanksby, S. Dua, J.H. Bowie, D. Schröder, H. Schwarz, J. Phys. Chem. 104 (2000) 11248.
[28] S.J. Blanksby, J.H. Bowie, Mass. Spectrom. Rev. 18 (1999) 181.
[29] C.A. Muedas, D. Sülze, H. Schwarz, Int. J. Mass Spectrom. 113 (1992) R17.
[30] A.M. McAnoy, S. Dua, J.H. Bowie, Org. Biomol. Chem. 2 (2004) 1742.
[31] Y. Sumiyoshi, H. Takada, Y. Endo, Chem. Phys. Lett. 387 (2004) 116.
[32] G.T. Yu, Y.H. Ding, X.R. Huang, G.H. Chen, A.C. Tang, J. Phys. Chem. A 108 (2004) 10723.
[33] H.L. Liu, X.R. Huang, G.H. Chen, Y.H. Ding, C.C. Sun, J. Phys. Chem. A 108 (2004) 11828.
[34] H.L. Liu, X.R. Huang, G.H. Chen, Y.H. Ding, C.C. Sun, J. Phys. Chem. A 108 (2004) 6919.
[35] N. Balucani, H.Y. Lee, A.M. Mebel, Y.T. Lee, R.I. Kaiser, J. Chem. Phys. 115 (2001) 5107.
[36] R.I. Kaiser, C. Ochsenfeld, M. Head-Gordon, Y.T. Lee, Astrophys. J. 510 (1999) 784.
[37] R.I. Kaiser, C. Ochsenfeld, M. Head-Gordon, Y.T. Lee, A.G. Suits, Science 274 (1996) 1508.
[38] R.I. Kaiser, D. Stranges, H.M. Bevsek, Y.T. Lee, A.G. Suits, J. Chem. Phys. 106 (1997) 4945.
[39] L.C.L. Huang, H.Y. Lee, A.M. Mebel, S.H. Lin, Y.T. Lee, R.I. Kaiser, J. Chem. Phys. 113 (2000) 9637.
[40] R.I. Kaiser, Y.T. Lee, A.G. Suits, J. Chem. Phys. 103 (1995) 10395.
[41] J.G. Mangum, A. Wootten, Astron. Astrophys. 239 (1990) 319.
[42] S. Yamamoto, S. Saito, H. Suzuki, S. Deguchi, N. Kaifu, S. Ishikawa, M. Ohishi, Astrophys. J. Part 1 348 (1990) 363.
[43] A. Van orden, J.D. Cruzan, R.A. Provencal, T.F. Giesen, R.J. Saykally, R.T. Boreiko, A.L. Betz, In Astronomical Society of the Pacific, Airborne Astronomy Symposium on the Galactic Ecosystem: From Gas to Stars to Dust, 73 (1995) 67.
[44] J. Cernicharo, J.R. Goicoechea, E. Caux, Astrophys. J. 534 (2000) L199.
[45] D. Fosse, J. Cernicharo, M. Gerin, P. Cox, Astrophys. J. 552 (2001) 168.
[46] K.H. Hinkle, J.J. Keady, P.F. Bernath, Science 241 (1988) 1319.
[47] S. Sebastian, N. Dieter, Astron. Astrophys. 336 (1998) 769.
[48] W. Huggins, Proc. R. Soc. London 33 (1882) 1.
[49] A.G. Lowe, A.T. Hartlieb, J. Brand, B. Atakan, K. Kohse-Hoinghaus, Combust. Flame 118 (1999) 37.
[50] M. Gerin, Y. Viala, F. Casoli, Astron. Astrophys. 268 (1993) 212.
[51] H.S. Liszt, B.E. Turner, Astrophys. J. Part 2 224 (1978) L73.
[52] L.M. Ziurys, D. McGonagle, Y. Minh, W.M. Irvine, Astrophys. J. Part 1 373 (1991) 535.
[53] M. Gerin, Y. Viala, F. Pauzat, Y. Ellinger, Astron. Astrophys. 266 (1992) 463.
[54] D. McGonagle, W.M. Irvine, Y.C. Minh, L.M. Ziurys, Astrophys. J. Part 1 359 (1990) 121.
[55] V.P. Gaur, Solar Phys. 46 (1976) 121.
[56] A.D. Becke, Phys. Rev. A 38 (1988) 3098.
[57] A.D. Becke, J. Chem. Phys. 98 (1993) 1372.
[58] A.D. Becke, J. Chem. Phys. 98 (1993) 5648.
[59] M.J. Frisch, G.W. Trucks, H.B. Schlegel, G.E. Scuseria, M.A. Robb, J.R. Cheeseman, V.G. Zakrzewski, J.A. Montgomery, Jr., R.E. Stratmann, J.C. Burant, S. Dapprich, J.M. Millam, A.D. Daniels, K. N. Kudin, M.C. Strain, O. Farkas, J. Tomasi, V. Barone, M. Cossi, R. Cammi, B. Mennucci, C. Pomelli, C. Adamo, S. Clifford, J. Ochterski, G.A. Petersson, P.Y. Ayala, Q. Cui, K. Morokuma, D.K. Malick, A.D. Rabuck, K. Raghavachari, J.B. Foresman, J. Cioslowski, J.V. Ortiz, B. B. Stefanov, G. Liu, A. Liashenko, P. Piskorz, I. Komaromi, R. Gomperts, R.L. Martin, D.J. Fox, T. Keith, M.A. Al-Laham, C.Y. Peng, A. Nanayakkara, C. Gonzalez, M. Challacombe, P.M.W. Gill, B. Johnson, W. Chen, M.W. Wong, J.L. Andres, C. Gonzalez, M. Head-Gordon, E.S. Replogle, J.A. Pople, GAUSSIAN 98 v A.7, Gaussian, Inc., Pittsburgh, PA, 1998.
[60] K. Fukui, Acc. Chem. Res. 14 (1981) 363.
[61] G.D. Purvis, R.J. Bartlett, J. Chem. Phys. 76 (1982) 1910.
[62] T.H. Dunning Jr, J. Chem. Phys. 90 (1989) 1007.
[63] I.W.M. Smith, E. Herbst, Q. Chang, Mon. Not. R. Astron. Soc. 350 (2004) 323.
[64] Z.Q. Zhu, Z.Q. Zhang, C.S. Huang, L.S. Pei, C.X. Chen, Y. Chen, J. Phys. Chem. A 107 (2003) 10288.
[65] J. Wang, Y.H. Ding, C.C. Sun, Chemphyschem 6 (2005) 431.
[66] H.E. Matthews, T.J. Sears, Astrophys. J. 272 (1983) 149.
[67] Y. Miao, D.M. Mehringer, Y.J. Kuan, L.E. Snyder, Astrophys. J. 445 (1995) L59.
[68] J. Cernicharo, M. Guelin, J.R. Parodo, Astrophys. J. 615 (2004) L145.
[69] N. Oliphant, A. Lee, P.F. Bernath, C.R. Brazier, J. Chem. Phys. 92 (1990) 2244–2247.